Received: 22 February 2024 | Revised: 22 April 2024 | Accepted: 16 May 2024

DOI: 10.1002/jbio.202400066

RESEARCH ARTICLE

JOURNAL OF BIOPHOTONICS

ATR-FTIR spectroscopy imaging of bone repair in mandibular laser-osteotomy

Carolina Benetti[1] | **Alberto Blay**[2] | **Luciana Correa**[3] | **Marco Aurelio Verlangieri**[3] | **Moisés O. dos Santos**[4] | **Sergei G. Kazarian**[5] | **Denise M. Zezell**[6]

[1]Center for Engineering, Modeling and Applied Social Sciences, Federal University of ABC, Santo André, Brazil

[2]Plenum Bioengineering, Jundiaí, Brazil

[3]Pathology Department, School of Dentistry, University of São Paulo, São Paulo, Brazil

[4]School of Technology, Amazonas State University, Manaus, Brazil

[5]Department of Chemical Engineering, Imperial College London, South Kensington Campus, London, UK

[6]Center for Lasers and Application, Instituto de Pesquisas Energéticas e Nucleares—IPEN/CNEN, São Paulo, Brazil

Correspondence
Denise M. Zezell, Center for Lasers and Applications, Instituto de Pesquisas Energéticas e Nucleares, IPEN/CNEN, São Paulo, São Paulo 055058-000, Brazil.
Email: zezell@usp.br

Funding information
FAPESP, Grant/Award Number: 21/00633-0; CNPq, INCT of Photonics, Grant/Award Number: 465763/2014-6; INCT of Radiation in Health Science, Grant/Award Number: 406761/2022-1; PQ, Grant/Award Number: 314517/2021-9; SWE, Grant/Award Number: 211210/2013-7; CAPES, Grant/Award Number: Finance code 001

Abstract

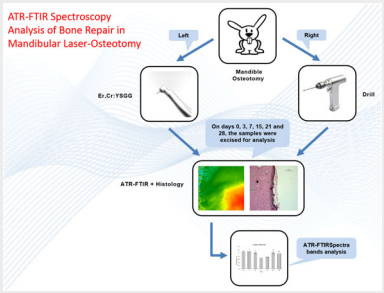

The aim of this study was to verify the effectiveness of attenuated total reflectance-fourier transform infrared (ATR-FTIR) spectroscopy in the characterization of bone repair in mandibular osteotomy using erbium, chromium-doped yttrium, scandium, gallium and garnet (Er,Cr:YSGG) laser and multilaminate drill on each side. Two mandible bone fragments were removed from 30 rabbits, and the process of bone repair was studied immediately, 3, 7, 15, 21, and 28 days after the surgery. The histological analysis allowed detecting differences in the early stages of tissue repair after bone cutting performed with the Er,Cr:YSGG laser or multilaminate drill. The ATR-FTIR spectroscopy technique was sensitive to changes in the organic content of bone tissue repair process.

KEYWORDS

ATR-FTIR, bone repair, Er,Cr:YSGG laser, histological analysis, multilaminated drill, osteotomy

1 | INTRODUCTION

Bone tissue is composed by mineral and organic matrices [1, 2]. The organic matrix is composed by cells (osteoblasts, osteocytes, and osteoclasts), protein fibers, and an aqueous gel-like amorphous substance named ground substance. The extracellular matrix (ECM) formed by fibrils of many collagen types, mainly type I, and along with ground substance is the major component of matrix [3].

Abbreviations: ATR-FTIR, attenuated total reflectance-fourier transform infrared spectroscopy; Er,Cr:YSGG, Erbium, chromium-doped yttrium, scandium, gallium and garnet.

The inorganic matrix is composed mainly by crystalline hydroxyapatite $\left[Ca_3(PO_4)_2\right]_3Ca(OH)_2$ and impurities which according to Legros et al. [4], lead to a general chemical formula, given by $Ca_{8.3}(PO_4)_{4.3}(HPO_4 or CO_3)_{1.7}\left(OH or \frac{1}{2}CO_3\right)_{1.7}$.

The healing process of bone is a sequence of stages consisting of four steps with considerable overlapping: hematoma formation, fibrocartilaginous callus formation, bone callus formation, and bone remodeling [5]. The magnitude of injury response is a competition of anabolic and catabolic responses process. A continuous process of resorption followed by replacement by new bone with little change in shape occur and is intensified after injury, facilitating the healing process [6].

Changes in amount of organic and mineral components in bone are important to evaluate mechanical and biochemical qualities of material formed due anabolic and catabolic processes and infrared spectroscopy is an important tool to characterize the bone matrix components. Fourier transform infrared (FTIR) spectroscopy provide valuable information from a semiquantitative and qualitative analyses of complex mixtures [7, 8]. Infrared spectra result from transitions between quantized vibrational energy states. The association of FTIR spectroscopy technique and array detectors (focal plane arrays [FPA] or linear arrays), allow simultaneous detection of spatially resolved spectra using a large number of small mercury cadmium telluride (MCT) detector elements [9]. The attenuated total reflectance (ATR) mode represents a complementary approach to the use of FTIR imaging, allowing to record chemical images at a spatial resolution with hundreds of data points per image pixel [10]. This reveal a biochemical fingerprint for mineral and organic identification and can be analyzed for information about the mineral structure.

The most frequently reported parameters of FTIR spectroscopy pertaining to bone material properties are (1) mineral-to-matrix ratio, (2) mineral maturity/crystallinity, and (3) collagen maturity [11–14].

The aim of this study was to verify the effectiveness of FTIR spectroscopy in the characterization of bone repair at different stages, after removing a fragment from the mandibular region using Erbium, chromium-doped yttrium, scandium, gallium and garnet (Er,Cr:YSGG) laser and multilaminate drill on each side.

2 | MATERIALS AND METHODS

2.1 | Animal model

This project was performed in partnership between the Center for Laser and Application—CLA—IPEN and the Imperial College of London and approved by the Ethics Committee on the Use of Animals from IPEN by No. 108/12—CEUA-IPEN. This project included 30 adult, male, New Zealand white rabbits, weighting about 3.0 to 4.0 kg, which were kept in individual cages throughout the trial period.

2.2 | Surgical procedure

The rabbits were anesthetized and submitted to wide submandible trichotomy. An intraoral incision was made in the periosteal region of the buccal sulcus, being exposed to the cortical bone plate. Bone fragments measuring approximately $7 \times 7 \times 3\ mm^3$ were removed causing a defect at the site. The bone cut was performed by an Er,Cr:YSGG laser ($\lambda = 2.79\ \mu m$) on the left side and the multilaminate drill on the right side. The Er,Cr:YSGG laser at $53\ J/cm^2$ of energy density with 80%:80% (water: air) was applied with fiber tip axial exchangeable, model/version MGG6 Sapphire (Biolase, Inc), with 0.4 mm length and 0.6 mm diameter. Before and after each surgery, the mean power was measure and energy density calculated was measured, and its value based on the literature and pilot studies. The multilaminate carbide drill was the FG 701, in high rotation. After the fragment was removed, the tissue was sutured in layers with absorbable thread. The euthanasia stage was performed on 0, 3, 7, 15, 21, and 28 days after surgical procedure [15]. Following that, two homologous samples were removed, one on each side of the mandible, with a safety margin and cleaned.

2.3 | Histological analysis

The bone fragments containing the region of interest were fixed in 10% formalin and submitted to steps for slides preparation for microscopic examination. The specimens were decalcified in ethylenediaminetetraacetic acid for 30 days and submitted to routine histological processing for paraffin embedding and hematoxylin–eosin staining. A single researcher evaluated qualitatively the histomorphological characteristics presented in Er,Cr:YSGG laser and drill groups.

2.4 | Spectroscopy analysis

2.4.1 | Sample preparation

To increase the contact sample-diamond in spectrometer the bone pieces were polished, to approximately 100 μm thick to minimize water influence on the infrared

absorption spectra [16], the samples were stored in a silica gel container for 96 h prior to measure. Samples of intact mandibular bone were prepared using the same protocol as the control group. Therefore, seven experimental groups were subjected to analysis using ATR-FTIR spectroscopy. These seven groups comprised six experimental groups associated with different stages of bone recovery, alongside a control group consisting of intact bone samples obtained from the corresponding anatomical region.

2.4.2 | Instrumentation

A FPA detector was used to obtain FTIR images with a Varian 670 FTIR spectrometer. It was coupled with ATR Specac Imaging Golden Gate™ system and a large sample compartment [17]. Spectra were collected with 4 cm^{-1} spectral resolution in 900–3800 cm^{-1} range with 64 scans. The FPA detector comprised 4096 small pixels arranged in a 64 × 64 grid format with each of the pixels measuring an infrared spectrum, thus acquiring 4096 spectra. The imaging area measured using this FPA detector was 780 μm × 610 μm. The ROI (region of interest), was selected for artifacts and paraffin removal, using CytoSpec (version 2.00.01).

2.4.3 | Spectral image processing

The first step was to truncate the fingerprint region: 900–1800 cm^{-1} for IR data analysis, for spectral artifacts (water and CO_2), and additional baseline distortions removal. Following, the spectral image was constructed using the intensity of the phosphate $\nu_1\nu_3$ band (900–1180 cm^{-1}). The ROI was selected in the images, and the other regions of the image were subtracted as shown in Figure 1.

For our analyses, we used the proportion between the bands, as is common in the analysis of mineralized tissues, and we took care to choose the maximum and minimum values of the color scale, according to the program's automatic default.

The analysis of overlapping bands, particularly in the region between 1250 and 1550 cm^{-1}, was conducted using the baseline method. This approach allowed for the selective analysis of prominent bands within the overlap.

In order to avoid errors using automatic area selection methods, not taking into account the variability of the spectra, a code developed in MatLab (MathWorks, USA) for baseline correction was applied. This code used a previously defined spectral interval to locate each band's starting and ending position and calculate the width, area, maximum intensity, and maximum position. The chosen bands for analysis points to isolate the band from the rest of the spectrum (r_1 and r_2), and other values used in the search for the starting and ending position of the band (p_1–p_4) are shown in the Table 1.

The code tests of the program were carried out with a set of 128 spectra extracted from a line of 2 × 64 pixels of the spectral image from a control group bone sample.

2.5 | Statistical analysis of band areas

For every sample, the ratio values of each image spectrum were computed, and the normality of the data was assessed through the Shapiro–Wilk test. As the ratio

TABLE 1 The bands analyzed with their respective boundaries, where r_1 and r_2: band choice; p_1 and p_2: points in the minimum region to the left of the band; p_3 and p_4: points in the minimum region to the right of the band.

Band	r_1–r_2 [cm^{-1}]	p_1–p_2 [cm^{-1}]	p_3–p_4 [cm^{-1}]
Amide I	1550–1750	1580–1600	1700–1720
Amide II	1480–1600	1505–1526	1575–1590
Carbonate	1250–1550	1270–1310	1515–1535
Amide III	1200–1350	1210–1230	1280–1310
Collagen	1140–1240	1165–1190	1205–1225
Phosphate	900–1200	900–910	1145–1158

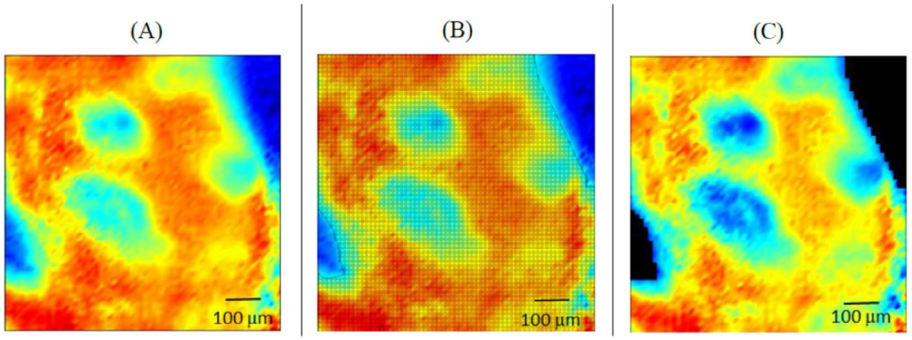

FIGURE 1 (A) Full image; (B) region of Interest selection; and (C) final image.

values passed the normality test in all samples, the proportion of the bands was depicted by the average ratio value of the various spectra comprising the spectral image.

At each stage of bone repair, the proportions of the bands between the experimental groups and the control group were compared when the cutting instrument was used: the Er,Cr:YSGG laser or multilaminated carbide drill at high speed. Due to the small number of samples per group, statistics were performed using the nonparametric Kruskal–Wallis test, with comparison between groups carried out with the Dunn's posttest, both with a significance of 0.05.

When comparing the stages of bone repair, we did not separate by cutting instrument, in order to increase the number of samples considered in each group. The comparison encompassed band area proportions across different stages of bone repair and the control group. Statistical analysis employed the non-parametric Kruskal–Wallis test and Dunn's posttest, with a significance level set at 0.05.

The normality of data for the width of the phosphate ν_1.

ν_3 band (around 1010 cm^{-1}) in the various spectra of each sample was confirmed using the Shapiro–Wilk test. The analysis focused on the average width of the phosphate spectra. Widths were compared across different repair stages and the control group, without differentiation based on the cutting instrument. Due to data consistency and dispersion, statistical analysis was conducted using ANOVA and Tukey's posttest, both with a significance level of 0.05.

3 | RESULTS AND DISCUSSION

3.1 | Histological evaluation

On zero day and day 7, the histological analysis showed a diffuse inflammatory infiltrate and slight thermal damage in region removed by the drill (Figure 2). No change was observed in the remaining bone adjacent to the cut interfaces. The specimens exposed to the Er,Cr:YSGG laser, presented thermal damage slightly greater than that observed in the drill group, as well as discrete inflammatory infiltrate. In both specimens, after 7 days, an immature granulation tissue was also noted in the cut interface region. In the early stages of bone repair, there are reports of delay in laser cutting compared to cutting with a drill [15, 18]. This delay is believed to occur due to the region of thermal necrosis caused by laser ablation, which demands a high resorption activity [19, 20].

On 15 and 21 days after surgery, a great amount of bone matrix deposition was observed in both cut methods, increasing the deposition area and the bone remodeling over the days. The presence of bone formation and remodeling can suggest that the thermal damage induced by Er,Cr:YSGG laser did not hinder the bone repair process [15, 21, 22].

On the last 2 days of follow-up, a trabecular pattern with greater cellularity and thickness was present in the histological sections of the two groups (Figure 3).

In this study, the necrotic zone observed after laser cut was smaller than 50 μm. Wang et al. used the Er,Cr:YSGG laser to perform a bone defect in the mandible region of adult rabbits, promoting localized thermal damage (with less than 100 μm) in both study regions. Seven days after surgery, it was not yet possible to observe major changes in the bone repair process, and only 14 days after surgery, granulation tissue with some ossification zones was identified [15].

Our results showed little faster repair process than Wang et al. when comparing the 14 days with 7 days. Despite this, our results suggest that the necrotic zone formed in the laser ablation process directly influences the speed of the bone repair [23, 24], although the laser-induced thermal damage was reduced in our specimens compared with the literature. This result reinforces the importance of selecting proper irradiation parameters when using the laser in surgical procedures.

3.2 | Spectroscopy analysis

The ATR-FTIR spectroscopy technique has been widely used in the characterization of mineralized tissue [14, 25, 26]; however, few studies have been carried out in an attempt to use this technique in the bone repair process characterization, knowing only that some of the characteristics of the infrared spectrum are associated with tissue maturity [16]. Consequently, the ATR-FTIR spectroscopy technique to characterize different stages of the bone repair process can provide new information about the structural and molecular changes that occur in the bone during this process.

The quality of the spectra obtained depends on technical factors, the sample preparation, and the standardization of the sample contact with the crystal [14]. In the standardization of an intensity scale, the phosphate band was used because it is more intense and stable, allowing the pressure control in the sample and allowing a high penetration of the evanescent wave, therefore a high absorption.

In the study, the bands of amide I, amide II, amide III, collagen, and phosphate were individually analyzed

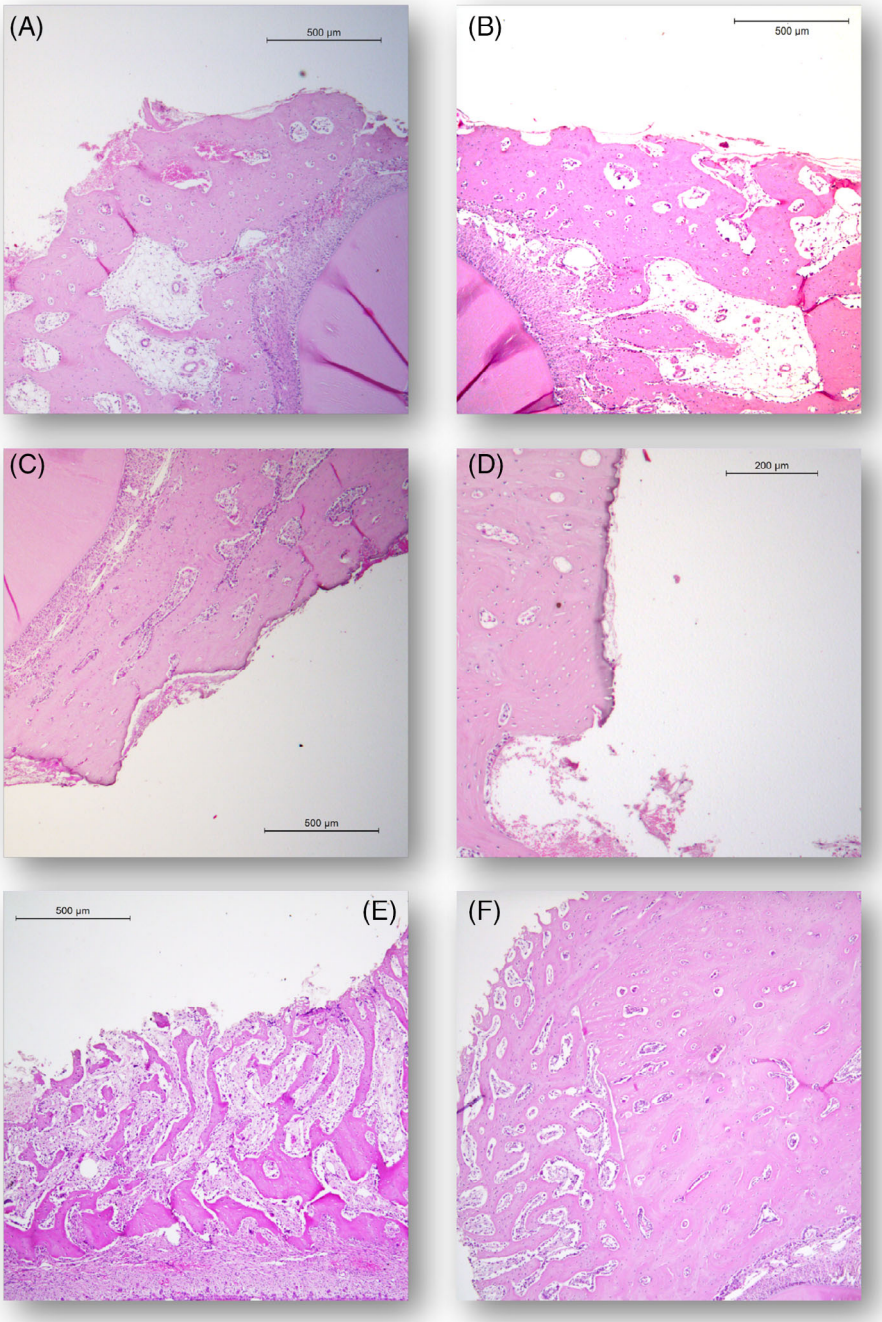

FIGURE 2 Rabbit mandible bone repair after osteotomy (HE) showing bone histological characteristics postsurgery, indicating a repair process with intense protein coagulation, suggesting thermal damage. Column: cut instrument: laser (left), drill (right); Row: follow-up days: 0D: A and B; 3D: C and D; 7D: E and F.

(Figure 4). The bands of carbonate and collagen were not analyzed individually due to the band overlapping, so in the study, they were analyzed as a single large band.

3.2.1 | Intensity versus band areas ratio

To ensure that the ratio between the spectrum bands area was not influenced by the intensity of the spectrum, a study of the intensity correlation of the amide II band with the phosphate-to-amide I bands ratio area.

The Spearman correlation coefficient showed that there is no correlation between the values of the spectra intensities and the value of the ratio between the areas of two bands ($r = -0.036$). This value ensures that the proportion between the areas of the bands is not affected by the difference in intensity of the spectra.

This proportion already excludes the possible differences in intensity between the spectra due to experimental factors, for example, the acquisition time of the spectrum concerning the background acquisition time.

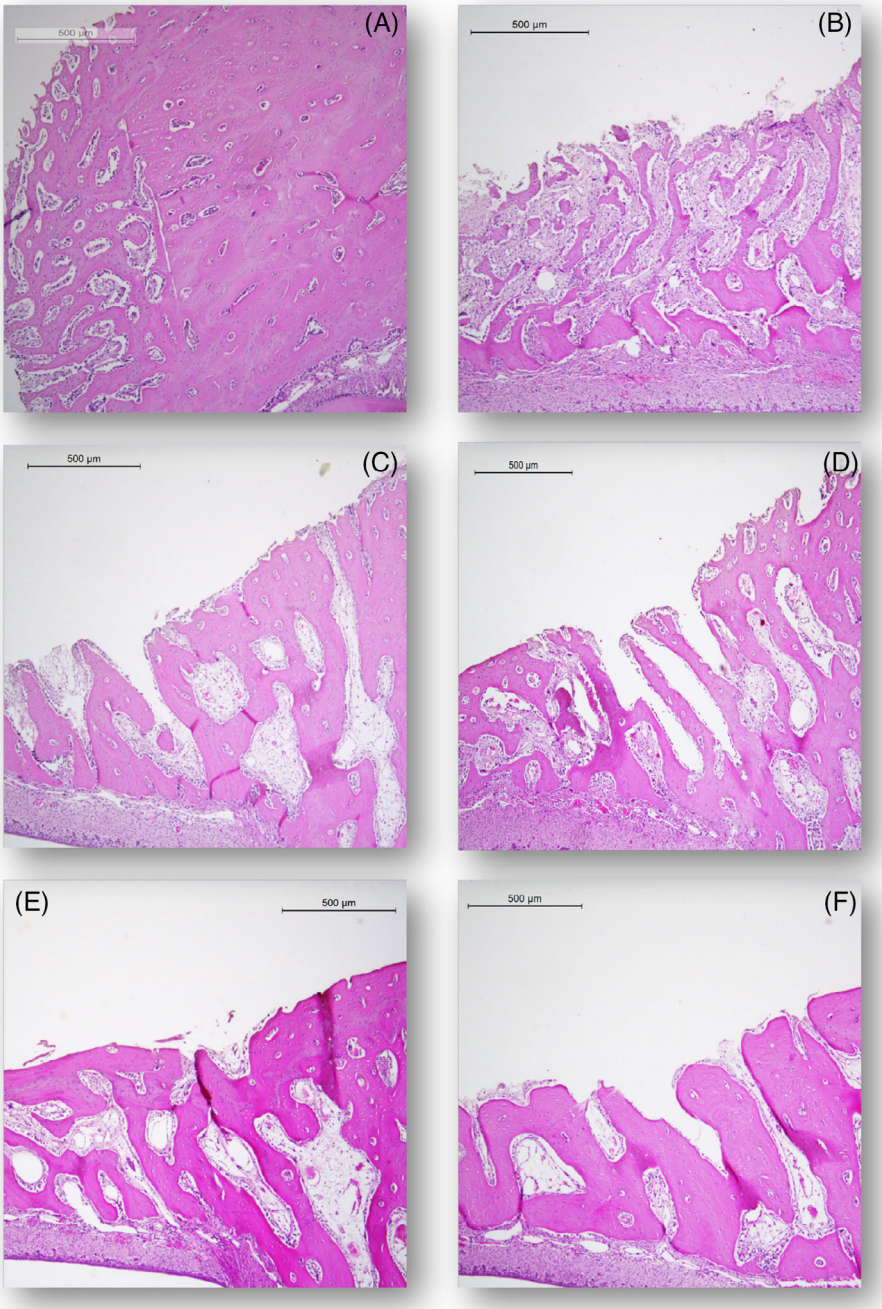

FIGURE 3 Histological sections from groups 15D, 21D, and 28D, showing the final stages of bone repair. Column: cut instrument: laser (left), drill (right); row: follow-up days: 15D: A and B; 21D: C and D; 28D: E and F.

3.2.2 | Ratio between band areas: Cutting instruments

To detect differences in the proportions and quantities of the components present in the sample [27–29], the ratio between the bands of the infrared spectrum was evaluated (Table 2). Phosphate band area was used in the normalization of the other areas because it is a very intense and defined band, which is not influenced by vibration modes from other compounds, therefore being exclusively related to the mineral part of the bone tissue.

The ratio between Amide I and Phosphate $\nu_1\nu_3$ band areas related to compounds of the organic matrix and mineral content is named the mineral-to-matrix ratio [30, 31]. The proportions between the areas of Amide III and collagen bands with area of phosphate band are also related to the organic content of mineralized tissues [27–29]. These compounds are less influenced by other absorption bands, as amide I and amide II than water and carbonate bands.

Bands of the mineral components, such as phosphate ν_4 (604 cm^{-1}) and the ratio between carbonate ν_2 (840–

890 cm^{-1}) and phosphate $\nu_1\nu_3$ bands important to evaluate the relative content of carbonate present in the sample were not analyzed due to the spectrophotometer detector specifications limited to the region from 4000 to 900 cm^{-1}.

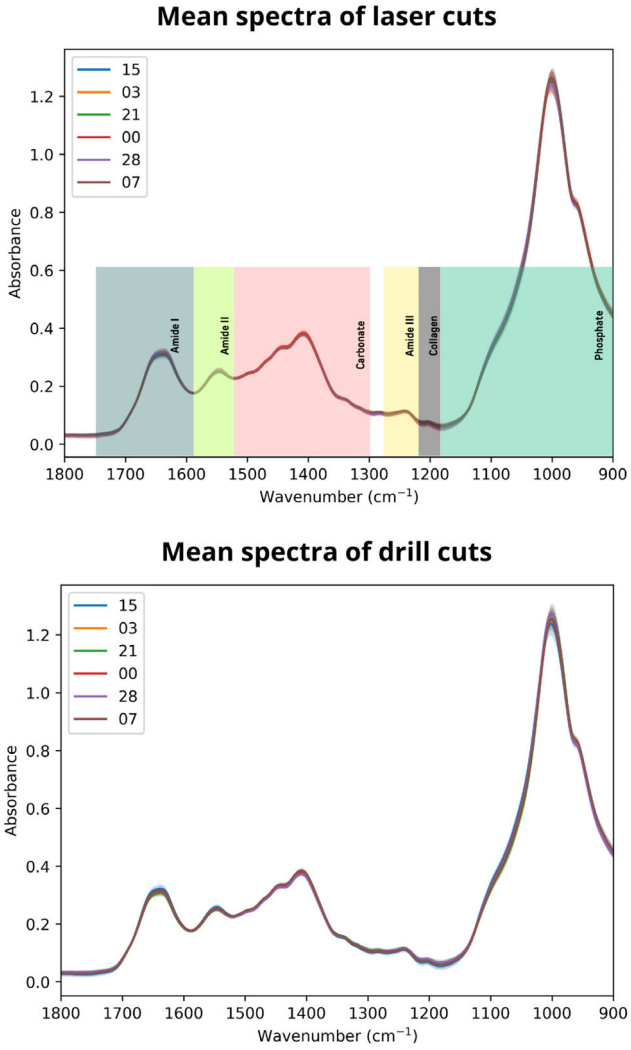

FIGURE 4 Mean spectra overlapping of each analyzed day groups. Upper image: laser cut spectra with analyzed bands; at the below: drill cut spectra.

TABLE 2 Bands evaluated for ratio determination.

Compound	Wavelength [cm^{-1}]
Phosphate $\nu_1\nu_3$	900–1150
Collagen	1210–1290
Amide III	1210–1290
Carbonate	1285–1520
Amide II	1510–1580
Amide I	1580–1710

The ratio of infrared bands area from groups: control, laser, and drill were compared in each bone restoration period, as shown in Figures 5–10. No statistically differences between the groups at any repair stage were observed as well as no trends in the bands' behavior.

In histological analysis, the laser caused a slightly greater thermal damage at cut interface than the drill, making it possible to observe at the histological cuts a necrosis area at the cut region up to 7 days after the surgical procedure. However, this difference was not observed in spectroscopic analyses, as shown in Figure 7. By histological and spectroscopic analysis, we found no significant differences between bone repair process of the laser group and drill group after 15 days of surgical procedure (Figures 8–10).

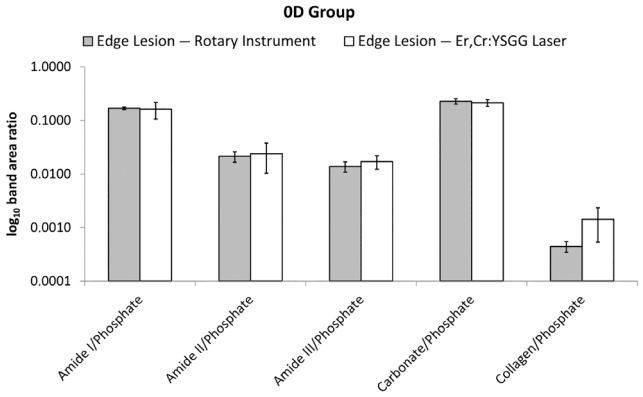

FIGURE 5 Zero-day analysis: Comparison between the laser and drill groups of the amide I / II and III, carbonate and collagen band areas ratio, normalized by the phosphate band for all days of the study. Er,Cr:YSGG, erbium, chromium-doped yttrium, scandium, gallium and garnet.

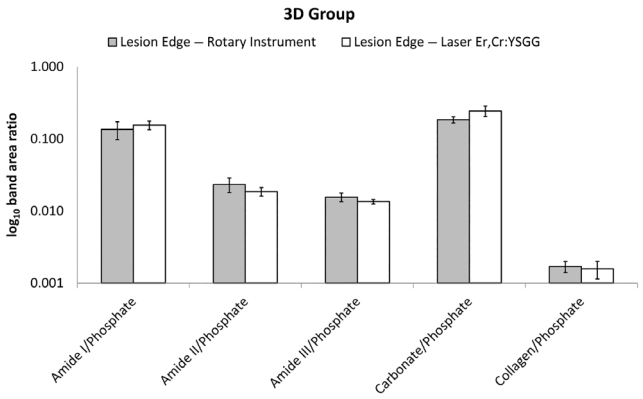

FIGURE 6 Third day analysis: Comparison between the laser and drill groups of the amide I / II and III, carbonate and collagen band areas ratio, normalized by the phosphate band for all days of the study. Er,Cr:YSGG, erbium, chromium-doped yttrium, scandium, gallium and garnet.

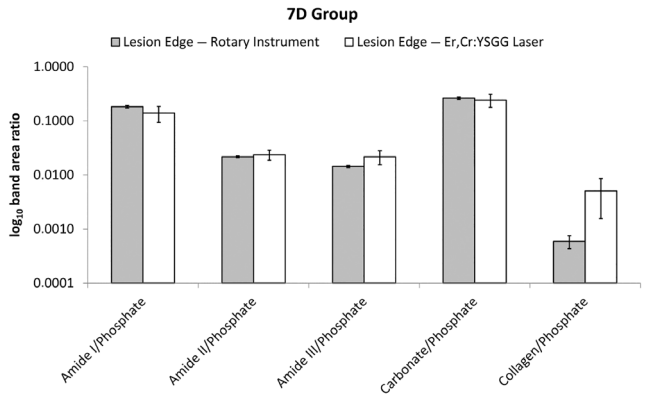

FIGURE 7 Seventh day analysis: Comparison between the laser and drill groups of the amide I/II and III, carbonate, and collagen band areas ratio, normalized by the phosphate band for all days of the study. Er,Cr:YSGG, erbium, chromium-doped yttrium, scandium, gallium and garnet.

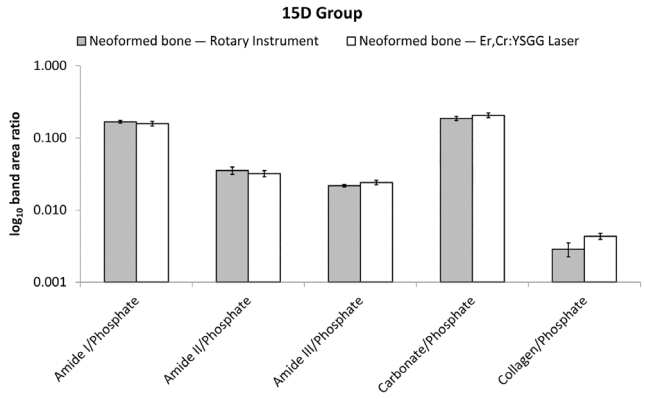

FIGURE 8 Fifteenth day analysis: Comparison between the laser and drill groups of the amide I/II and III, carbonate, and collagen band areas ratio, normalized by the phosphate band for all days of the study. Er,Cr:YSGG, erbium, chromium-doped yttrium, scandium, gallium and garnet.

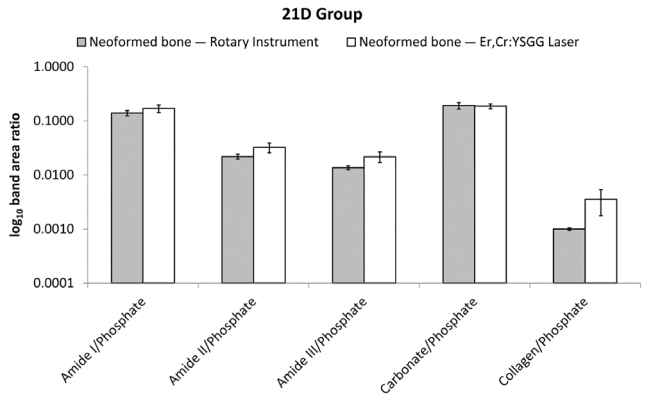

FIGURE 9 Twenty-first day analysis: Comparison between the laser and drill groups of the amide I/II and III, carbonate and collagen band areas ratio, normalized by the phosphate band for all days of the study. Er,Cr:YSGG, erbium, chromium-doped yttrium, scandium, gallium and garnet.

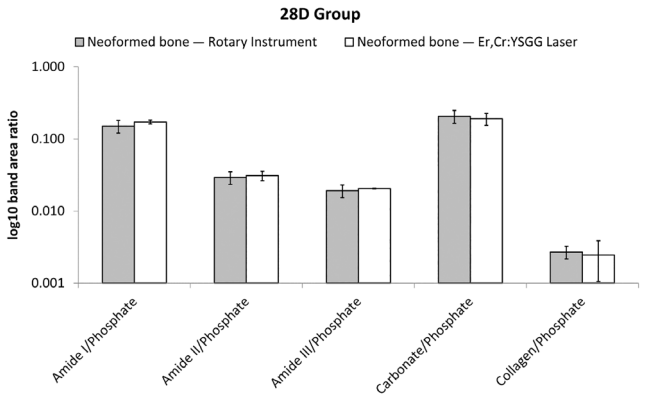

FIGURE 10 Twenty-eighth day analysis: Comparison between the laser and drill groups of the amide I/II and III, carbonate, and collagen band areas ratio, normalized by the phosphate band for all days of the study. Er,Cr:YSGG, erbium, chromium-doped yttrium, scandium, gallium and garnet.

The study of infrared proportion spectrum bands was not effective in demonstrating the influence of different cutting tools in the bone repair process. The heterogeneity of bone tissue and the total of samples used may have contributed to the result obtained. In an attempt to show the differences observed in the histological analysis, multivariate data analysis can be applied for the recognition of a chemical structure class of bone chemical compounds. Therefore, the potential of the ATR-FTIR spectroscopy technique in differentiating the effects of different tools cutting in the bone repair process cannot be ruled out.

3.2.3 | Ratio between band areas: Repair stages

The proportion of bone tissue components at different repair stages in relation to the control bone was evaluated. Considering the reduced number per group sample in the previous analysis, the data were regrouped without distinction between the cutting tool used during surgery (rotary instrument or Er,Cr:YSGG laser).

The phosphate-to-amide I bands ratio at the different stages of bone repair and the control group showed no statistical significant difference (Figure 11). It is known that this ratio tends to decrease with the maturity of the tissue [16]. The downward trend in the collagen maturity, which is represented by the phosphate-to-amide I ratio, was not observed in analysis.

It is interesting to highlight that the amide I band is overlapped on a water vibration mode, making it difficult to determine the influence of each compound on the bands behavior. To minimize this, interference samples

were kept in a humid environment with controlled temperature until 96 h before the analysis, then desiccated with silica to keep standard hydration. However, the samples were not fully dehydrated, and it is possible that amide I band analysis was affected by the water band. Studies involving the irradiation of bone tissue samples with the Er,Cr:YSGG laser showed that amide I band presents an intermediate behavior between the water band and the organic compounds [27], due to the influence that water has on the behavior of this band.

The phosphate-to-amide II and phosphate-to-amide III band area ratio in the different stages of the repair plus the control group were represented on the Figure 12 which shows their similar behavior. For reasons of scale, the ratio values for each band were normalized to their respective maximum value. This analysis revealed a statistical difference between the 15 days group and control group in both bands.

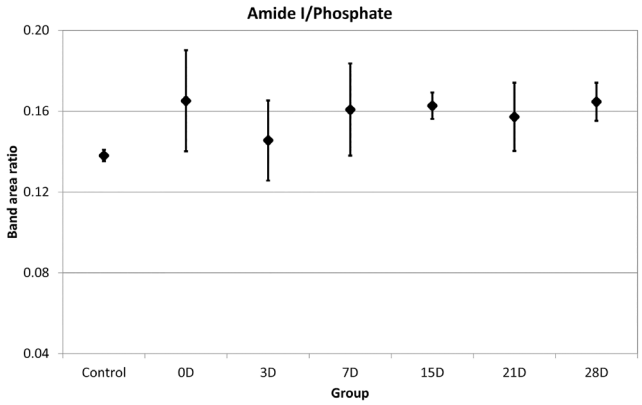

FIGURE 11 Phosphate-to-amide I bands ratio: Mean values of the bands areas ratio in the different repair stages and in the control group. The bars error correspond to standard error of the data mean.

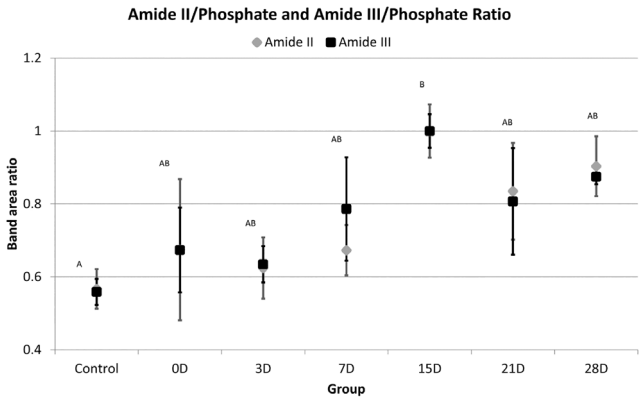

FIGURE 12 Phosphate-to-amide II/III bands ratio: Mean values of the bands areas ratio in the different repair stages and in the control group. The bars error correspond to standard error of the data mean.

As mentioned previously, the proportions between the amide II and amide III bands areas concerning the phosphate band area are also related to the organic content of mineralized tissues [27–29]. As can been seen in Figure 12 the proportion of organic content in the samples gradually increased from the 3 to the 15 day, when it reached its peak, decreasing in the more advanced stages of the repair process.

This tendency supports what was observed in histological analyzes, in which it was found that 3 to 15 days after the surgical procedure, granulation connective tissue is formed in the lesion region. From the fifteenth day onwards, the mineralization of this matrix began to occur more intensely.

A tendency in the ratio between the organic matrix and the mineral content observed in the analyzed amide II and amide III bands suggests ATR-FTIR spectroscopy technique as sensitive to changes in organic content in the bone tissue repair process. It was also observed in the study of the collagen band, as can be observed in Figure 13, although no statistically significant differences were observed between the different stages of the bone repair process.

An analysis of the ratio between the carbonate and phosphate bands was also carried out (Figure 14). There was no statistical difference or tendency between the data. The carbonate band (1410–1445 cm^{-1}) and the collagen band at 1335 cm^{-1} exhibited overlap, making it difficult to distinguish them individually in the spectra obtained from a sample. Instead, they frequently appeared as a single broad band. In previous studies, Benetti [32] evaluated these bands separately, producing consistent findings, unlike the scenario observed for other collagen and carbonate bands across various spectral regions. The result is expected because this region

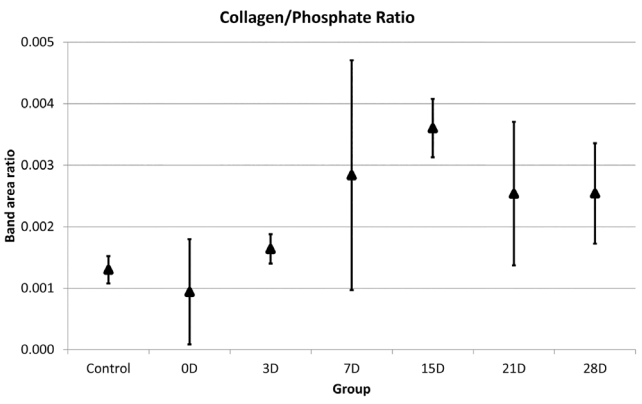

FIGURE 13 Phosphate-to-collagen bands ratio: Mean values of the bands areas ratio in the different repair stages and in the control group. The bars error correspond to standard error of the data mean.

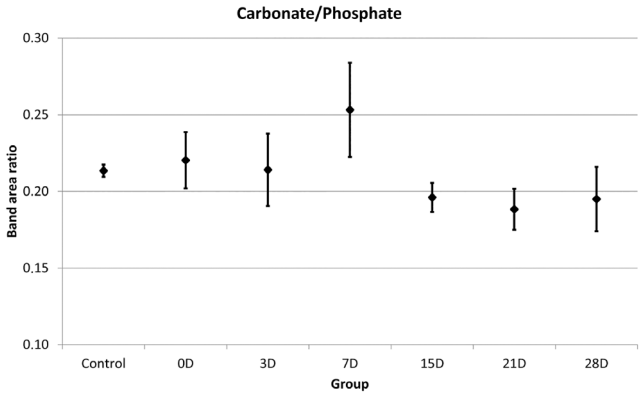

FIGURE 14 Phosphate-to-carbonate bands ratio: Mean values of the bands areas ratio in the different repair stages and in the control group. The bars error correspond to standard error of the data mean.

has overlapping modes of organic vibration, mineral, and water components, making it difficult to observe the behavior of any of these components using solely this band.

In response to visualization difficulties, it was decided to consider the carbonate and collagen bands together as a unified broadband for analysis.

It was verified at histological analysis that the bone cut performed with the Er,Cr:YSGG laser promoted a slight thermal damage in the remaining tissue (<50 μm). The literature suggests that the necrotic zone observed in the Laser Group is due to an increase in temperature above 150°C [33]. This increase is high enough to promote degradation of organic compounds in bone tissue [34]. However, there were no differences between the control group and the zero-day group results by spectroscopic analysis, even when only laser group was considered.

The ATR-FTIR technique has already proved effective in detecting changes in mineralized tissues caused by the increase in temperature. Studies that used the ATR-FTIR technique to evaluate dentin subjected to different temperature increments showed that a temperature raise of 150°C was sufficient to cause a 50% reduction of the compound band areas value located between 1150 and 1350 cm^{-1} (amide III and collagen) [35]. The technique has also proven effective in detecting variations caused by the irradiation of the Er,Cr:YSGG laser in bones, dentin, and enamel [27, 29, 36, 37].

One hypothesis for the lack of trends in zero-day group is related to selection of the region of interest in the spectral images, which may have considered a region larger than the thermal damage zone. According to histological analysis, thermal damage caused by the cutting instruments to the tissue was discrete, and the bone tissue adjacent to the interface did not exhibit morphological changes. Therefore, when selecting the region of interest, spectra related to the adjacent tissue (not affected during bone cutting) may have been considered in the analysis, which would hinder the differentiation of the groups. This hypothesis is reinforced by the error bar obtained in each group. Note that the latter is higher in the laser group and drill group, compared with the control group, indicating a greater dispersion of data in these groups.

3.3 | Phosphate bandwidth

The phosphate $\nu_1\nu_3$ band plays an important role in spectroscopic analysis of mineralized tissue, not only because it is a well-defined and intense band but also because it is related to several properties of bone tissue, such as maturity, crystallinity, and phosphoric acid content. In this band region, several sub-bands generated by the phosphate ions are found, such as the one centered on 1030 cm^{-1}, related to the asymmetric stretching of the phosphate (ν_3PO_4) mode of vibration associated with nonstoichiometric apatite located at 1120 cm^{-1} [38].

The phosphate sub-bands analysis is used to determine the crystallinity and maturity indexes of bone tissue; however, it is difficult to accurately determine their amount and location of them. Paschalis et al. used the second derivative spectrum and determined 11 peaks in the phosphate $\nu_1\nu_3$ (900–1180 cm^{-1}), band spectrum [39]; however, this method is questionable about its stability and reproducibility [40]. The most used process is to decompose the phosphate $\nu_1\nu_3$ band domain into five sub-bands (1110, 1082, 1060, 1030, and 962 cm^{-1}) [41, 42]. However, Rey et al. demonstrated a variation in the position, intensity, and quantity of bands according to the mineralized tissue, its stage of maturity, and even the environment in which the spectral measurements are performed [43].

Since it is difficult to identify and separate the sub-bands of the phosphate $\nu_1\nu_3$, it was decided to study its bandwidth in a first analysis. The bandwidth is associated with the vibration modes that compose, and therefore, a change in the phosphate bandwidth may indicate a change in crystallinity and maturity.

The Figure 15 shows the values with statistical differences of the ratio between the areas of the collagen and phosphate bands in the different stages of bone repair and in a control bone. In it is shows that phosphate bandwidth gradually decreases up to 7 days after the surgical procedure, and slowly increase after this period. Histological analysis showed that between 7 and 15 days after the surgical procedure, the process of bone matrix deposition by osteoblasts is already underway, after 21 days of

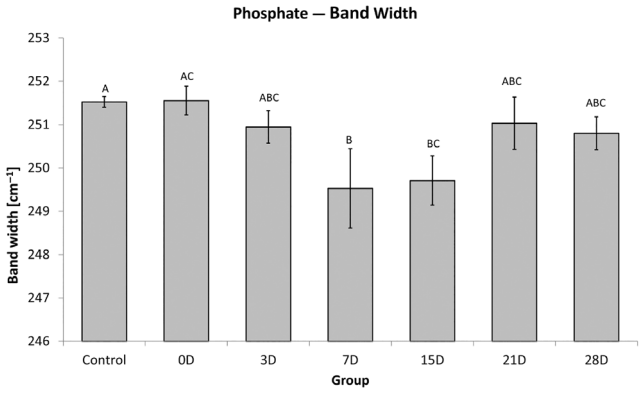

FIGURE 15 Mean values of phosphate-to-collagen band areas ratio in the different stages of repair and control group. Distinct letters differs statistically by the Tukey test.

surgery, the mineralization of the samples gradually increases. The similarities between the behavior observed in Figure 15 and the results of the histological analysis suggest that the width of the phosphate band is related directly to the degree of mineralization of bone tissue.

The maturity index is calculated using the sub-bands area ratio located at 1030 and 1010 cm^{-1} [40]; however, only with the width of the phosphate band, nothing can be inferred about the behavior of the sub-bands. In contrast, maturity is related to the proportion of apatite and nonapatite domains in the tissue structure, which tends to increase with the tissue mineralization process. Thus, the results indicate that the phosphate bandwidth is related to tissue maturity.

Further studies are needed to confirm whether the phosphate bandwidth is related to tissue maturity. The observed results showed that the width of the phosphate $\nu_1\nu_3$ band is related to the mineralization of the samples, reinforcing the ATR-FTIR spectroscopy as a technique to characterize the bone repair process.

4 | CONCLUSION

The acquisition and analysis protocols developed were effective in obtaining the spectral images of the different bone repair stages.

The results indicate that the ATR-FTIR spectroscopy technique is able to characterize the different stages of bone repair. There was a current toward an increase in the proportion of organic compounds up to 15-day group, after which there was an increase in the proportion of inorganic compounds indicating high mineralization after this period, which is corroborated by histological analysis. However, with the analysis techniques used, it was not yet possible to detect differences regarding the cutting instrument used (Er,Cr:YSGG laser or multilaminate drill).

ACKNOWLEDGMENTS

The authors would like to thank the following funding: FAPESP 21/00633-0. CNPq (INCT of Photonics 465763/2014-6, INCT of Radiation in Health Science 406761/2022-1, PQ 314517/2021-9 and SWE 211210/2013-7) and CAPES: Finance code 001.

CONFLICT OF INTEREST STATEMENT

The authors declare no conflicts of interest.

DATA AVAILABILITY STATEMENT

The data that support the findings of this study are available from the corresponding author upon reasonable request.

ORCID

Luciana Correa https://orcid.org/0000-0002-5774-0750
Moisés O. dos Santos https://orcid.org/0000-0003-0050-0876
Sergei G. Kazarian https://orcid.org/0000-0003-1768-9134
Denise M. Zezell https://orcid.org/0000-0001-7404-9606

REFERENCES

[1] N. Reznikov, M. Bilton, L. Lari, M. M. Stevens, R. Kröger, *Science* **2018**, *360*, eaao2189.
[2] K. Grandfield, V. Vuong, H. P. Schwarcz, *Calcif. Tissue Int.* **2018**, *103*, 606.
[3] R. E. Burgeson, M. E. Nimni, *Clin. Orthop. Relat. Res.* **1992**, *282*, 250.
[4] R. Legros, N. Balmain, G. Bonel, *Calcif. Tissue Int.* **1987**, *41*, 137.
[5] A. Schindeler, M. M. McDonald, P. Bokko, D. G. Little, *Semin. Cell Dev. Biol.* **2008**, *19*, 459.
[6] J. Burch, S. Rice, H. Yang, A. Neilson, L. Stirk, R. Francis, P. Holloway, P. Selby, D. Craig, *Health Technol Assess* **2014**, *18*, 1.
[7] P. A. Castro, C. A. Lima, M. R. Morais, T. M. Zorn, D. M. Zezell, *Appl. Spectrosc.* **2020**, *74*, 758.
[8] M. O. D. Santos, A. Latrive, P. A. A. de Castro, W. de Rossi, T. M. T. Zorn, R. E. Samad, A. Z. Freitas, C. L. Cesar, N. D. V. Junior, D. M. Zezell, *Biomed. Opt. Express* **2017**, *8*, 1575.
[9] S. G. Kazarian, K. A. Chan, *Analyst* **2013**, *138*, 1940.
[10] G. Steiner, E. Koch, *Anal. Bioanal. Chem.* **2009**, *394*, 671.
[11] E. P. Paschalis, R. Mendelsohn, A. L. Boskey, *Clin. Orthop. Relat. Res.* **2011**, *469*, 2170.
[12] W. L. Randle, J. M. Cha, Y. S. Hwang, K. A. Chan, S. G. Kazarian, J. M. Polak, A. Mantalaris, *Tissue Eng.* **2007**, *13*, 2957.
[13] B. Gieroba, A. Przekora, G. Kalisz, P. Kazimierczak, C. L. Song, M. Wojcik, G. Ginalska, S. G. Kazarian, A. Sroka-Bartnicka, *Mater. Sci. Eng., C* **2021**, *119*, 111634.
[14] N. Shanas, W. Querido, J. Oswald, K. Jepsen, E. Carter, C. Raggio, N. Pleshko, *Appl. Spectrosc.* **2022**, *76*, 416.

[15] X. Wang, C. Zhang, K. Matsumoto, *Lasers Med. Sci.* **2005**, *20*, 21.
[16] A. Boskey, N. P. Camacho, *Biomaterials* **2007**, *28*, 2465.
[17] S. G. Kazarian, K. A. Chan, *Appl. Spectrosc.* **2010**, *64*, 135A.
[18] J. S. Nelson, A. Orenstein, L. H. L. Liaw, M. W. Berns, *Lasers Surg. Med.* **1989**, *9*, 362.
[19] M. A. El Montaser, H. Devlin, P. Sloan, M. R. Dickinson, *Lasers Surg. Med.* **1997**, *21*, 255.
[20] R. C. Nuss, R. L. Fabian, R. Sarkar, C. A. Puliafito, *Lasers Surg. Med.* **1988**, *8*, 381.
[21] X. Wang, N. T. Ishizaki, N. Suzuki, Y. Kimura, K. Matsumoto, *J. Clin. Laser Med. Surg.* **2002**, *20*, 245.
[22] L. R. Perussi, C. Pavone, G. J. P. L. de Oliveira, P. S. Cerri, R. A. C. Marcantonio, *Lasers Med Sci* **2012**, *27*, 95.
[23] K. Yoshida, K. Uoshima, K. Oda, T. Maeda, *Clin. Oral Implants Res.* **2009**, *20*, 782.
[24] A. R. Eriksson, T. Albrektsson, B. Albrektsson, *Acta Orthop. Scand.* **1984**, *55*, 629.
[25] C. C. A. Lopes, P. H. J. O. Limirio, V. R. Novais, P. Dechichi, *Appl. Spectrosc. Rev.* **2018**, *53*, 747.
[26] M. Figueiredo, J. Gamelas, A. Martins, *Infrared Spectroscopy-Life and Biomedical Sciences*, INTECHopen, Rijeca, Croatia **2012**, p. 315.
[27] C. Benetti, M. O. dos Santos, P. A. da Ana, L. Bachmann, D. M. Zezell, *Biomed. Spectrosc. Imaging* **2014**, *3*, 301.
[28] L. Bachmann, A. S. Gomes, D. M. Zezell, *Spectrochim. Acta, Part A* **2005**, *62*, 1045.
[29] D. Zezell, P. Ana, C. Benetti, V. Goulart, L. Bachmann, C. Tabchoury, J. A. Cury, *Lasers in Dentistry XVI*, Vol. 7549, International Society for Optics and Photonics, Bellingham-WA **2010**, 75490G.
[30] D. Faibish, A. Gomes, G. Boivin, I. Binderman, A. Boskey, *Bone* **2005**, *36*, 6.
[31] A. L. Boskey, R. Mendelsohn, *J. Biomed. Opt.* **2005**, *10*, 031102.
[32] C. Benetti, Study of bone repair by ATR - FTIR spectroscopy technique after the removal of a fragment from jaw region using Er,Cr:YSGG laser or drill. **2010**. https://doi.org/10.11606/T.85.2014.tde-30092014-104657
[33] H. Kang, J. Oh, A. Welch, *Phys. Med. Biol.* **2008**, *53*, 3381.
[34] L. Bachmann, A. S. Gomes, D. M. Zezell, *Spectrosc. Lett.* **2004**, *37*, 565.
[35] L. Bachmann, O. Baffa, D. Zezell, *Philos. Mag.* **2007**, *87*, 1033.
[36] C. Benetti, M. O. Santos, J. S. Rabelo, P. A. Ana, P. R. Correa, D. M. Zezell, *Photonic Therapeutics and Diagnostics VII*, Vol. 7883, International Society for Optics and Photonics, Bellingham- WA **2011**, p. 78834P.
[37] P. Ana, C. Kauffmann, L. Bachmann, L. Soares, A. Martin, A. Gomes, D. M. Zezell, *Laser Phys.* **2014**, *24*, 035603.
[38] J. D. Termine, A. S. Posner, *Nature* **1966**, *211*, 268.
[39] E. Paschalis, E. DiCarlo, F. Betts, P. Sherman, R. Mendelsohn, A. Boskey, *Calcif. Tissue Int.* **1996**, *59*, 480.
[40] D. Farlay, G. Panczer, C. Rey, P. D. Delmas, G. Boivin, *J. Bone Miner. Metab.* **2010**, *28*, 433.
[41] B. R. Wood, L. Chiriboga, H. Yee, M. A. Quinn, D. McNaughton, M. Diem, *Gynecol. Oncol.* **2004**, *93*, 59.
[42] N. Pleshko, A. Boskey, R. Mendelsohn, *Biophys. J.* **1991**, *60*, 786.
[43] C. Rey, M. Shimizu, B. Collins, M. J. Glimcher, *Calcif. Tissue Int.* **1990**, *46*, 384.

How to cite this article: C. Benetti, A. Blay, L. Correa, M. A. Verlangieri, M. O. dos Santos, S. G. Kazarian, D. M. Zezell, *J. Biophotonics* **2024**, *17*(9), e202400066. https://doi.org/10.1002/jbio.202400066